

# Measuring Influenza A Virus and Peptide Interaction Using Electrically Controllable DNA Nanolevers

Marlen Kruse,\* Christin Möser, David M. Smith, Hanna Müller-Landau, Ulrich Rant, Ralph Hölzel, and Frank F. Bier

Electrically controllable deoxyribonucleic acid (DNA) nanolevers are used to investigate the binding interaction between Influenza A/Aichi/2/1968 and the peptide called “PeB”, which specifically binds the viral surface protein hemagglutinin. PeB is immobilized on gold electrodes of a “switchSENSE” biochip by conjugation to DNA-strands that are hybridized to complementary anchors. The surface-tethered DNA strand carries a fluorophore while the complementary strand is a multivalent arrangement carrying up to three PeB peptides. The nanolevers are kept upright (static) by applying a negative potential. Signal read-out for this static measurement mode is the change in fluorescence intensity due to changes in the local environment of the dye upon binding. Measurements of virus-peptide interaction show that the virus material specifically binds to the immobilized peptides and remains bound throughout the measurement time. Immobilized viruses are subsequently used as ligands to characterize oligovalent peptide binding to hemagglutinin, revealing rate constants of the interaction. Moreover, three Influenza A subtypes are compared in their binding behavior. Overall, this paper shows the ability to immobilize virus material on a sensor surface, which allows to target virus-proteins in their native environment. The “switchSENSE” method is therefore applicable to characterize virus-receptor interactions.

A comparable pandemic was caused by an influenza A virus in 1918 called the Spanish flu,<sup>[2]</sup> that resulted in millions of deaths throughout the world.<sup>[2]</sup> Influenza A viruses still account for annual epidemics of varying severity.<sup>[3]</sup> Recently in 2009, the world was faced with the swine flu, an influenza A virus.<sup>[2]</sup>

Influenza A is a virus of the Orthomyxoviridae family and is enveloped by a lipid bilayer that carries three membrane proteins: hemagglutinin (HA) and neuraminidase (NA), as well as the M2 proton channel.<sup>[4]</sup> Neuraminidase is required for the release of the virus particles from infected cells and cleaves the glycoside link.<sup>[5]</sup> Hemagglutinin attaches to the sialic acid (SA) containing cell receptors on the host cell prior to viral fusion. It has a homotrimeric structure carrying three SA binding sites on its globular head domain HA1.<sup>[6]</sup> The affinity of hemagglutinin to individual sialic acid is in the millimolar range,<sup>[7]</sup> but it is abundantly available on the virus surface and can interact with multiple SA residues on the cell surface to result in


a high overall avidity.<sup>[6,8]</sup> Kinetic characterization of affinity and avidity rate constants of multiple receptor binding to hemagglutinin is of vast interest to understand virus internalization and virus infection. Due to this complex binding process, it is desirable to expand the available measurement techniques like, for

## 1. Introduction

Viral pandemics pose a significant threat to mankind as has been shown again by the recent outbreak of the coronavirus severe acute respiratory syndrome coronavirus 2 (SARS-CoV-2).<sup>[1]</sup>

M. Kruse, R. Hölzel  
Fraunhofer IZI-BB  
Am Mühlenberg 13, 14476 Potsdam, Germany  
E-mail: marlen.kruse@izi-bb.fraunhofer.de

M. Kruse, C. Möser, F. F. Bier  
University of Potsdam  
Am Neuen Palais 10, 14469 Potsdam, Germany

 The ORCID identification number(s) for the author(s) of this article can be found under <https://doi.org/10.1002/admt.202101141>.

© 2021 The Authors. Advanced Materials Technologies published by Wiley-VCH GmbH. This is an open access article under the terms of the Creative Commons Attribution-NonCommercial-NoDerivs License, which permits use and distribution in any medium, provided the original work is properly cited, the use is non-commercial and no modifications or adaptations are made.

The copyright line for this article was changed on 8 November 2021 after original online publication.

DOI: 10.1002/admt.202101141

C. Möser, D. M. Smith  
Fraunhofer IZI  
Perlickstraße 1, 04103 Leipzig, Germany

D. M. Smith  
University of Leipzig  
Peter Debye Institute for Soft Matter Physics  
Linnéstr. 5, 04103 Leipzig, Germany

D. M. Smith  
University of Leipzig  
Medical Faculty  
Institute of Clinical Immunology  
Liebigstr. 18, 04103 Leipzig, Germany  
H. Müller-Landau, U. Rant  
Dynamic Biosensors GmbH  
Lochhamer Strasse 15, 82152 Martinsried/Planegg, Germany  
R. Hölzel  
Free University Berlin  
14195 Berlin, Germany

example, surface plasmon resonance,<sup>[9]</sup> nuclear magnetic resonance,<sup>[10]</sup> or electrical detection<sup>[11]</sup> for virus-receptor interactions.

In this work, fluorescence proximity sensing of the “switchSENSE” technology (static mode) was used to measure binding kinetics of hemagglutinin on the viral surface to a receptor. This technology is based on an electrically controllable DNA monolayer on a metal surface enabling measurements of kinetic rates.<sup>[12–16]</sup> It has been applied to determine binding affinity constants of a large variety of molecular interactions, for example, for protein–protein,<sup>[17]</sup> aptamer–protein,<sup>[18]</sup> or DNA–protein<sup>[19]</sup> interactions. Prior to this work, this technology has not been used for the assessment of viral properties and their interaction with receptors. We show that it is possible to expand the range of applications of switchSENSE technology to virus–peptide interactions. Finding complementary measurement techniques to the ones that exist today can expand the understanding of the inherent complexity of binding affinity interaction measurements.

One of the significant capabilities of the switchSENSE technology is the possibility to not only determine dissociation constants ( $K_D$ ) but also rate constants ( $k_{on}$  and  $k_{off}$ ). These kinetic parameters are increasingly considered to be highly relevant for the efficacy of candidates in drug discovery.<sup>[20,21]</sup> Other measurement techniques available determine dissociation constants ( $K_D$  values) but lack the ability to resolve binding kinetic parameters. Examples for these are microscale thermophoresis (MST),<sup>[22]</sup> radioligand binding assays,<sup>[23]</sup> or isothermal calorimetry (ITC).<sup>[23]</sup> Furthermore, there are methods, which are based on diffusion time variations upon a binding event like fluorescence correlation spectroscopy (FCS)<sup>[24]</sup> or fluorescence anisotropy (FA).<sup>[25]</sup> These are able to determine kinetic parameters but require fluorescent labeling of one of the binding partners, which is not necessary in switchSENSE. Binding can also be observed in enzyme-linked immunosorbent assays (ELISA). These are easy to handle, inexpensive, and have a high throughput,<sup>[26]</sup> but rate constants can not be determined.

One technique that enables the real-time measurement of kinetic parameters is surface plasmon resonance (SPR).<sup>[27]</sup> switchSENSE technology is comparable to SPR measurements since it has several similar advantages as well as obstacles. A similar nomenclature is therefore adopted. Some advantages of SPR as well as switchSENSE lie in i) the aforementioned measurability of kinetic parameters in real time, ii) label-free detection, iii) low sample consumption, and iv) high sensitivity of the technique.<sup>[27,28]</sup> Disadvantages the two techniques share lie in i) necessary immobilization of one of the interaction partners and therefore possible influence on binding behavior, ii) mass transport limitations, and iii) non-specific binding. Furthermore, miss or over interpretation of data is a possible pitfall. SPR and switchSENSE both require experience and expertise to operate the device and evaluate the data.<sup>[27–30]</sup>

A main advantage of switchSENSE technology compared to SPR lies in the controllable receptor surface. switchSENSE sensor surface allows placing ligands at a defined density, reducing crowding and allowing to distribute two different ligands at a customized ratio to mimic cooperative effects. Further, the generic sensor surface can be used for various types of interactions as it utilizes an immobilization method based on reversible DNA hybridization. switchSENSE is especially

advantageous when the receptor of interest is DNA-based, like the DNA-peptide nanoconstructs in our case. These are particularly easy to immobilize and analyze. Additionally, switchSENSE technology can be used to measure conformational changes<sup>[31]</sup> as well as hydrodynamic radii,<sup>[32]</sup> which is not possible in SPR.

There have been reports on measuring dissociation of virus particles from receptors by probing single virions either by single-molecule force spectroscopy<sup>[33]</sup> or total internal reflection microscopy (TIRF).<sup>[34]</sup> These techniques are beneficial for understanding individual interactions but describe a principally distinct approach from the averaged signal collection that is utilized in SPR, MST or switchSENSE.

The peptide called “PeB” was derived from the complementary determining region of the variable domain ( $V_H$ ) of the immunoglobulin heavy chain of monoclonal antibody HC19, which is known to have neutralizing effects on influenza strain hemagglutinin 2 neuraminidase 3. It was previously shown to bind the HA protein of influenza A virus Aichi H3N2, with an affinity in the micromolar range in the monomeric form.<sup>[35]</sup> While this interaction is several orders of magnitude stronger than the monovalent affinity between HA and SA, and indeed does inhibit infection of cells in the mid-micromolar range, a large amount of improvement and optimization would be needed for this to even approach the efficacy necessary for therapeutic development.

To this end, a number of approaches used the concepts of templated multivalence<sup>[36]</sup> in order to amplify the effect of small ligands targeting single, biological receptor complexes. For the influenza HA receptor, the binding sites for the natural ligand sialic acid are arranged in a well-defined homotrimer, with approximately 4.2 nm between neighboring sites.<sup>[37]</sup> In several cases, DNA- or other nucleotide-based nanostructures have been used as convenient, biocompatible structural scaffolds for presenting HA-binding ligands in a geometrically complementary bi.<sup>[38]</sup> or trivalent arrangement,<sup>[39–41]</sup> thus enhancing both overall binding strength, and the ability to inhibit agglutination of red blood cells by the virus particles. Two recent patent filings<sup>[42,43]</sup> have also extended this concept to the DNA-based templating of peptide-based viral inhibitors, where the peptide PeB used in this present study was reported to prevent agglutination of red blood cells by influenza A at a concentration approximately 250 times lower than the monovalent peptide by itself.<sup>[42]</sup> While data on the inhibition of infection was not reported for this particular peptide-virus pair, a significant 500-fold enhancement of a peptide designed to block the major receptor responsible of the fusion of respiratory syncytial virus (RSV) was shown,<sup>[43]</sup> indicating the potential value of this approach.

A second convenience of using DNA or other DNA-compatible polymers that obey Watson–Crick base-pairing is that their integration onto substrates for many types of analytical assays is straightforward. By extending unpaired, single-stranded sequences from structures, these can act as simple and modular and, at the same time, reversible anchor points to complementary sequences on the analytical surface. This is especially advantageous for methods such as the one we report here, which is based upon the dynamic motion of double stranded DNA (dsDNA) nanolevers in oscillating electric fields. Here, we present, for the first time, interaction studies of virus

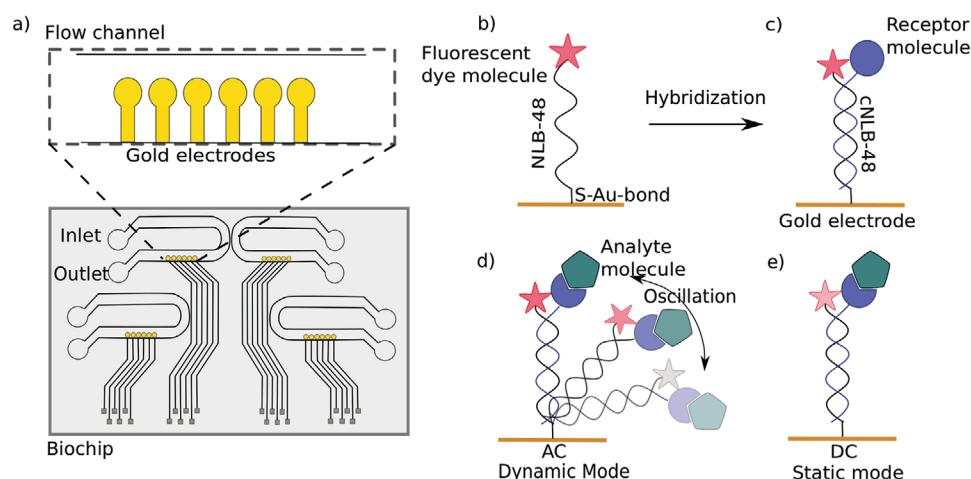


**Figure 1.** a) Top view of a switchSENSE microfluidic biochip with four flow channels. Each channel comprises six gold electrodes. The more detailed view shows the six independent measurement electrodes in a row within the microfluidic channel. b) Schematic overview of a single stranded DNA nanolever (NL-B48) immobilized on a gold electrode via thiol coupling. The nanolever carries a fluorophore at the lateral end. c) The DNA monolayer is functionalized with the ligand of interest by hybridization of the complementary DNA strand carrying a receptor molecule at the distal end. d) Dynamic measurement mode: The double stranded DNA nanolever is actuated to a switching motion by applying an alternating potential. The fluorescence signal is gradually quenched by energy transfer upon approaching the gold surface. Read-out of this mode is the switching speed of DNA nanolevers. The switching speed is slowed down upon binding of an analyte to the ligand molecule adding friction to the nanolever. e) Static measurement mode: DNA nanolevers are kept at an upright position. Read-out of this mode is the change in fluorescence intensity upon binding of an analyte due to changes in the local environment of the dye. Drawings are not to scale.

particles with artificial peptide-DNA-nanoconstructs applying switchSENSE technology.

## 2. Experimental Section

### 2.1. Measuring system

Binding interaction measurements were performed with switchSENSE technology using a DRX<sup>2</sup> device (Dynamic Biosensors GmbH, Germany). Standard multipurpose biochips MPC2-48-1-R1-S or MPC2-48-2-G1R1-S were used for measurements (Dynamic Biosensors GmbH). The microfluidic biochips comprise four independent flow channels (see Figure 1a). Each channel has a width of 1 mm, a height of 60  $\mu\text{m}$ , and contains six gold electrodes in series over a length of 3.34 mm, which have a diameter of 120  $\mu\text{m}$  and are connected to a voltage source.

An indium tin oxide (ITO) coating at the channel's upper surface is used as counter electrode. Each electrode is equipped with a monolayer of DNA nanolevers. Single stranded DNA nanolevers (NL-B48, sequence can be found in Table 1) are covalently attached at the 5' end to the electrode surface via a gold-sulfur bond and carry a fluorescent molecule at the 3' end. The complementary DNA strand (cNL-B48, sequence in Table 1) can be crosslinked with a receptor molecule of interest via coupling chemistry. In this case, a peptide was crosslinked to the complementary DNA strand via click chemistry (see Section 2.2). Functionalization of the sensor surface was obtained by on-chip hybridization of the complementary DNA-peptide conjugate to the surface-tethered DNA strands. The rigid double-stranded and functionalized DNA nanolevers on the gold electrode can be manipulated electrically. The gold electrodes are connected to a voltage source that can produce either an alternating

voltage (AC) or a direct voltage (DC) which corresponds to the two switchSENSE measurement modes, namely "dynamic mode" (AC voltage) and "static mode" (DC voltage). For the dynamic mode, AC voltages in the range between  $-0.3\text{ V}$  and  $0.5\text{ V}$  at frequencies up to 10 kHz can be applied. Because of the intrinsically negatively charged DNA backbone, a positive voltage will result in an attractive force and a negative voltage in a repulsive force. An alternating voltage will therefore lead to an oscillation of the end-tethered DNA nanolever.

When measuring in dynamic mode, the fluorescence signal is quenched gradually due to energy transfer to the gold surface when a positive voltage is applied and the fluorophore approaches the electrode. The motion of the DNA with attached fluorophore triggered by the AC voltage results in a periodic variation of the detected intensity of emitted light from the

**Table 1.** Oligonucleotide sequences used for DNA trimers.

Name	Sequence 5' $\rightarrow$ 3'
NL-B48	TAGTCGTAAGCTGATATGGCTGATTAGTCGGAAGCATCGAACGCTGAT
cNL-B48	ATCAGCGTTCGATGCTTCCGACTAATCAGCCATATCAGCTTACGACTA
p-cNL-B48	ACACACACAACTAATCAGCGTTCGATGCTTCCGACTAATCAGC-CATATCAGCTTACGACTA <sup>a)</sup>
n	ATTAGTTTCTATCA
n*o	TGATAGAACTAAATATAATATGCGAGCCA <sup>a)</sup>
o*p*	TGGCTCGCATATTATTAGTTGTGTGTGT <sup>a)</sup>

The cNL-B48 part is complementary to the NL-B48 sequence used on the measurement chips in the DRX<sup>2</sup>. n and n\* are partially complementary, as well as o and o\* and p and p\*.

<sup>a)</sup>These sequences were modified with an aminolink C6 at the 5' end.

fluorophores. The emitted light is detected in real-time via electrically triggered time correlated single photon counting (E-TCSPC) coupled to the voltage generator. In case of a binding event, the hydrodynamic friction of the levers is increased resulting in a slower motion of the DNA nanolever. This specific change in nanolever switching speed can be detected in real-time. The signal is averaged over the whole electrode.

The static measurement mode uses constant negative voltages (in this case  $-0.1$  V) leading to an upright position of the DNA nanolever. Filter units in front of the detector unit ensures the detection of emission and suppression of excitation light. In static mode, the change in fluorescence light emission intensity is attributed to changes in the close chemical proximity of the fluorescent dye molecule. This mode does not depend on the size of the analyte as it is only sensitive to the chemical environment of the binding sites. Depending on the type of interaction, the binding event can result in an increase or a decrease in fluorescence intensity.<sup>[46]</sup>

## 2.2. DNA Nanoconstructs

The DNA constructs were synthesized based on the DNA sequences in Table 1.

DNA strands cNL-B48 and NL-W48-B48-G1 were purchased from Dynamic Biosensors GmbH, Martinsried, Germany. Oligonucleotides p-cNL-B48, n, n\*o, and o\*p\* in Table 1 were purchased from Biomers.net (Germany) and resuspended in ultrapure water. The sequence p-cNL-B48 was chosen to be partially complementary to the 48 bases of the immobilized NLB-48 strand. Oligonucleotides carrying amino groups (p-cNL-B48, n\*o, o\*p\*) were functionalized with peptide PeB according to.<sup>[47]</sup> In brief, oligonucleotides were incubated with a 100-fold molar excess of dibenzocyclooctyne N-Hydroxy-succinimide (DBCO-NHS) ester (Jena Bioscience, Germany) in 1x PBS pH 7.4. The reaction was left at room temperature overnight and was purified the next day via ethanol precipitation. Azide-modified peptide PeB was dissolved in ultrapure water and drops of 0.1 M sodium hydroxide were added until the turbid solution turned clear. Afterward, the dissolved peptide was added at 10- to 20-fold molar excess to DBCO-modified oligonucleotides. The reaction was incubated at room temperature overnight. Next, PeB-functionalized oligonucleotides were folded into a four-arm structure (see Figure 2). For optimal stoichiometry and high yields, all strands were mixed in equimolar amounts in PCR tubes. For DNA structures carrying 0, 1, 2, or 3 peptides, PeB-modified DNA strands were replaced by 3, 2, 1, or 0 unmodified strands, respectively. The mixture of oligonucleotides was supplemented with PBS pH 7.4 and structures were folded using a thermocycler (Biomera, Germany). At the beginning, the mixture was heated to  $\geq 90$  °C to denature secondary structures and nonspecific base pairing. For specific base pairing, the reaction was incubated at 54 °C for 15 min, followed by incubation at 30 °C for 5 min, and then further cooled to 4 °C. Amicon Ultra centrifugal filters with 30 K molecular weight cut-off (EMD Millipore, Germany) were used to isolate modified DNA constructs from unbound peptides. Coupling of peptides to oligonucleotides was evaluated prior to the binding measurements by native polyacrylamide gel electrophoresis

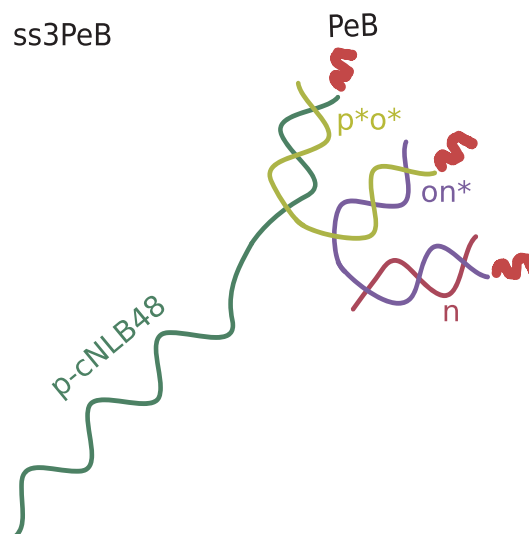


**Figure 2.** Schematic view of the nanoconstruct ss3PeB (not drawn to scale). The single stranded overhang is complementary to NL-B48 on the electrode surface.

(see Supporting Information). The peptide-presenting DNA construct has a molecular mass of approximately 43 kDa, when unmodified and a molecular mass of 49 kDa when functionalized with three peptides.

## 2.3. Peptides

The peptide sequence called PeB was taken from Memczak et al.<sup>[35]</sup> ARDFYDYDVFFYAMD-amide (PeB). The peptide was modified with azidobutyric acid at the N-terminal and has a molecular weight of 1995 Da. It was synthesized by Peptide Speciality Laboratories GmbH, Heidelberg, Germany. PeB was derived from the complementary determining region of the antibody HC19.

## 2.4. Virus Material

All virus material was provided by the Robert Koch Institute in Berlin, Germany. The virus samples were purified by density gradient centrifugation, inactivated by  $\beta$ -propio-lactone inactivation, and stored in PBS-Buffer at  $-80$  °C.

Prior to use of the virus material in the binding assay, the sample was vortexed for 2 min. Dilutions were prepared using PE140 buffer (10 mM  $\text{Na}_2\text{HPO}_4/\text{NaH}_2\text{PO}_4$ , 140 mM NaCl, 0.05% Tween 20, 50  $\mu\text{M}$  EDTA, 50  $\mu\text{M}$  EGTA).

A/Aichi/2/1968 (H3N2), also called X31 had an initial protein concentration of 1.4 g L<sup>-1</sup>, A/California/7/2009 (H1N1) of 1 g L<sup>-1</sup> and A/Panama/2007/1999 of 1.15 g L<sup>-1</sup> determined by BCA-Test.

## 2.5. Binding Assays

Binding assays were performed using a DRX<sup>2</sup>(Dynamic Biosensors GmbH, Martinsried, Germany). Standard multipurpose



biochips MPC-48-1-R1-S or MPC2-48-2-G1R1-S were used for measurements (Dynamic Biosensors GmbH). They were used according to the manufacturer's instructions. PE40 (10 mM  $\text{Na}_2\text{HPO}_4/\text{NaH}_2\text{PO}_4$ , 40 mM NaCl, 0.05% Tween 20, 50  $\mu\text{M}$  EDTA, 50  $\mu\text{M}$  EGTA) was used as auxiliary buffer as recommended by the manufacturer. As running buffer, PE140 (10 mM  $\text{Na}_2\text{HPO}_4/\text{NaH}_2\text{PO}_4$ , 140 mM NaCl, 0.05% Tween 20, 50  $\mu\text{M}$  EDTA, 50  $\mu\text{M}$  EGTA) was used. Complementary DNA strands (such as cNL-B48) were purchased from Dynamic Biosensors GmbH, as well as regeneration solution and glass vials. All consumables were used according to the manufacturer's instructions. Measurement protocols were established using the switchBUILD software and carried out using switchCONTROL software (both provided by Dynamic Biosensors GmbH). Each flow channel was passivated prior to measurements using a thiol-containing passivation solution (Dynamic Biosensors GmbH). Afterward, the electrode that showed the highest fluorescence amplitude in the chip status test was selected for further measurements. One flow channel was typically used for up to four measurement cycles. Immobilization of the DNA constructs was done by conjugate hybridization using a concentration of 500 nM for an on-chip hybridization time of 320 s. Interaction measurements were carried out in static mode. Analyte concentration ranged from 10 to 40  $\mu\text{g mL}^{-1}$ . All data were acquired with the system temperature set to 25 °C. For the association process, an analyte volume of 50  $\mu\text{L}$  and a flow speed of 1  $\mu\text{L min}^{-1}$  for 50 min were chosen. If not otherwise stated, a dissociation volume of 40  $\mu\text{L}$  with a flow speed of 3  $\mu\text{L min}^{-1}$  for 13.3 min was used. After measurements, a standby routine was performed to store the biochip with double stranded DNA.

## 2.6. Sandwich Assay

For the sandwich assay the DNA strand NL-W48-B48-G1 (Dynamic Biosensors GmbH) was used, which is partially complementary to the cNL-B48 part of the DNA nanoconstruct. This sequence is tagged with a green fluorescence molecule (G1) optimized for detection in the DRX<sup>2</sup>. Both DNA constructs (NL-W48-B48-G1 and DNA nanoconstruct ss1/2/3PeB) were hybridized in solution prior to the binding assay. This step was performed as a simple labeling strategy of the DNA nanoconstruct ss1/2/3PeB with a green fluorescent dye. Both constructs were mixed at a 1:1 ratio (v/v) (20  $\mu\text{L}$  of 1  $\mu\text{M}$  each) in a glass vial and incubated for 1 h at room temperature in the dark. In the switchBUILD kinetics set up, the capture immobilization method was selected to perform a sandwich assay. The peptide ss2PeB was set as ligand, the virus X31 was set as capture, and the peptide-DNA construct ss1/2/3PeB-NL-W48-B48-G1 was set as analyte. For the capture reaction, X31 was injected at a concentration of  $c = 40 \mu\text{g mL}^{-1}$ , with an association volume of 50  $\mu\text{L}$  and a flow rate of 1  $\mu\text{L min}^{-1}$ . The temperature was set to 25 °C. For the analyte interaction measurement, 40  $\mu\text{L}$  of ss1/2/3PeB-NL-W48-B48-G1 was injected at different concentrations. The association flow rate was set to 3  $\mu\text{L min}^{-1}$ . For dissociation, a volume of 10 mL buffer was pumped with a flow rate of 500  $\mu\text{L min}^{-1}$  for 20 min using the peristaltic pump of the DRX<sup>2</sup> device. All measurement steps were carried out in static mode.

## 3. Results and Discussion

### 3.1. Binding Interaction of X31 and PeB

The interaction measurement is based on the immobilization of double stranded DNA nanolevers on gold electrodes in a microfluidic environment. One of the single strands of the DNA (NL-B48) is attached to the electrode surface at the 5' end via thiol coupling and carries a fluorophore at the 3' end for optical detection. The complementary strand allows functionalization with a receptor molecule. The resulting double stranded DNA is intrinsically negatively charged and can be manipulated electrically. An alternating voltage applied to the gold electrode results in an oscillation of the end-tethered DNA strand (measurement mode called "dynamic mode"), while applying a direct voltage leads to a static situation in which the DNA nanolever stands upright (measurement mode called "static mode"). In both cases, the fluorophore's emission carries information about the binding event. For the dynamic mode, the speed of the DNA nanolever's motion is slowed down due to higher hydrodynamic friction after a binding event, resulting in a delay between the optical and the electrical signal. For the static mode, a binding event leads to a change in the light emission intensity due to a variation of the chemical environment in close proximity to the fluorophore (fluorescence proximity sensing). In our case, the hybridization of the DNA nanoconstructs is carried out in dynamic mode (see Figure 3a), while all virus binding interaction measurements are carried out in static mode. This means that after hybridization a DC voltage is applied, which results in an upright and static position of the DNA-peptide constructs. Virus binding is then observed by fluorescence proximity sensing. For our purpose, the complementary second DNA strand has a four-armed structure. One arm is partially complementary to the NL-B48 single stranded DNA (ssDNA) on the gold electrode. The other three arms can be functionalized to carry the peptide PeB each. The azide based copper free click chemistry conjugation leaves the binding ability of the peptide to hemagglutinin intact, as determined by microscale thermophoresis. The constructs ss1PeB, ss2PeB, ss3PeB, and ss0PeB carry one, two, three, and no peptides each, respectively. Figure 3b shows real-time hybridization of cNL-B48 and of ss3PeB to the immobilized NL-B48 strand on the biochip. An alternating voltage is applied during hybridization inducing a switching behavior of the DNA nanolevers. Prior to injection of the complementary strands, the ssDNA on the electrode surface oscillates only weakly due to the flexible structure of the single strand. Thus, the end-tethered fluorophore remains close to the surface resulting in low fluorescence amplitude signal. Upon injection of the complementary DNA strands (Figure 3,  $t = 20$  s), hybridization can be followed in real-time by a significant increase in switching amplitude as rigid double-stranded nanolevers push the fluorophore further away from the surface.<sup>[19]</sup> The detected fluorescence amplitude signal is averaged over the whole electrode surface, reaching saturation after sufficient surface functionalization.

Figure 3 shows that hybridization of the DNA construct ss3PeB to NL-B48 occurs faster as compared to the bare complementary DNA strand cNL-B48. This is not an intuitive finding, as one would expect a larger molecule to diffuse more

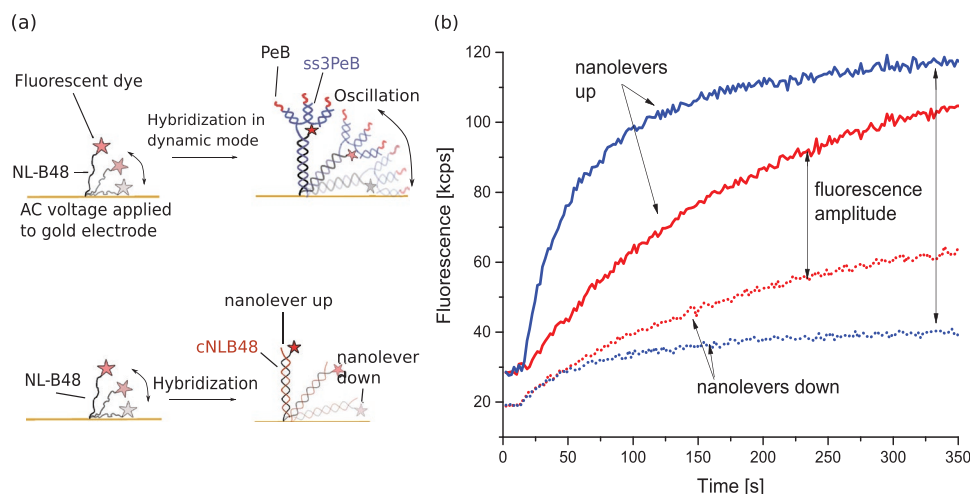


**Figure 3.** a) Schematic overview of the on-chip hybridization process of ss3PeB-cNLB48 and cNLB48 onto NL-B48-R1 nanolevers on the sensor surface. b) DNA nanolevers are set into a high frequency switching motion while the fluorescence intensity is observed in real-time. The fluorescence amplitude is defined as the difference of the obtained signal when DNA nanolevers are standing upright (solid lines) and when lying down (dotted lines).  $0 < t < 20$  s: Oscillation of single stranded DNA nanolevers.  $t > 20$  s: Complementary strands are injected and dsDNA nanolevers are formed by hybridization. Subsequent surface functionalization of bare cNL-B48 DNA (red trace) and ss3PeB construct (blue trace) are shown in one plot.

slowly to the surface in comparison to the bare cNL-B48 single strand. Additionally, ss3PeB comprises relatively long double stranded parts and thus carries more negative charges than cNL-B48, increasing repulsion between ss3PeB and NL-B48. One reason for faster hybridization times could be an enhanced attraction of the negatively charged construct towards the charged surface.

After functionalization of the surface with ss2PeB (or ss1PeB, ss3PeB, respectively), the virus solution was injected for virus association. Virus binding to ss2PeB is depicted schematically in **Figure 4**. A minimal fluid flow was necessary to guarantee that the reaction is not limited by diffusion. Based on

the model of Squires et al.,<sup>[48]</sup> a flow rate of  $1 \mu\text{L min}^{-1}$  was calculated to be sufficient. All virus-binding measurements were carried out in static mode. Since nanolever length is approximately 20 nm and the average virus diameter is around 120 nm for spherical particles and over 300 nm for rod shaped particles,<sup>[4]</sup> an oscillation of this DNA nanolever after virus capture appears impossible. Furthermore, a single virus particle can bind to more than one nanolever at the standard nanolever surface density further impeding DNA switching. In static mode, nanolevers are kept at an upright position and change in fluorescence signal obtained in close proximity to the interaction is recorded.<sup>[49]</sup>

**Figure 5** shows X31 virus binding onto a ss2PeB functionalized surface for three different concentrations of X31 from 10 to  $40 \mu\text{g mL}^{-1}$ . Upon injection of X31 virus solution, association can be observed by a concentration dependent decrease of fluorescence intensity.

After each measurement, the surface was regenerated and new ss2PeB nanostructures were immobilized. The dissociation curves show that over the measurement time of 750 s, the virus material mostly remained stable on the sensor surface. At first sight, this might be surprising with a published dissociation constant in the  $\mu\text{M}$  range.<sup>[35]</sup> However, this value was found for the monovalent interaction between free peptide and immobilized HA on the SPR surface and therefore excludes any multivalent binding effects. In our setup, virus particles are employed instead of recombinant protein and it is expected that one virus particle binds to more than one nanoconstruct on the surface. With an average lateral distance of 50 nm between nanoconstructs and a virus diameter of 120 nm to 300 nm,<sup>[4]</sup> one virus particle is expected to bind from five to seven nanoconstructs on average. This stabilizes the virus capture dramatically, as all bound nanoconstructs have to dissociate simultaneously for complete virus dissociation. If only one pair of interaction partners unbinds, rebinding will occur as the virus is still bound to the surface increasing local concentration

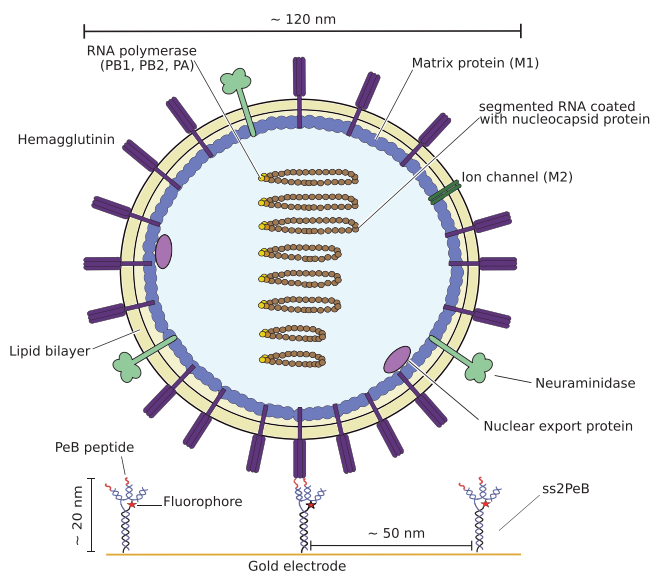


**Figure 4.** Schematic illustration of one Influenza A virus X31 binding to the peptides attached to DNA nanoconstructs (here shown for ss2PeB). The virus is captured on the sensor surface by specific interaction of hemagglutinin to the presented peptide construct. Schematic is drawn to scale.

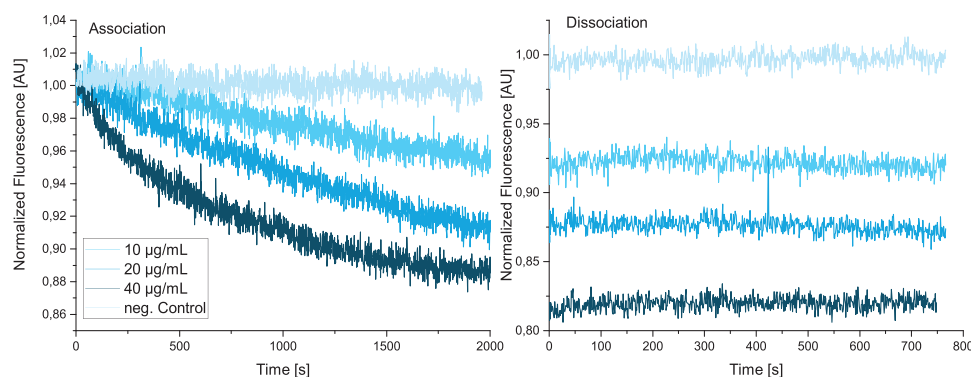


**Figure 5.** Binding of X31 virus via hemagglutinin - ss2PeB interaction. Concentration-dependent decrease in fluorescence signal due to virus binding. Sensor surface was functionalized with fresh ss2PeB constructs for each virus injection. X31 virus solution was injected at three different protein concentrations, 10, 20, and 40  $\mu\text{g mL}^{-1}$ . For the negative control, DNA constructs without peptides were immobilized and 40  $\mu\text{g mL}^{-1}$  virus solution was injected. The dissociation traces show that the virus material remains attached to the sensor surface.

of available hemagglutinin proteins (avidity effect). These effects of oligovalent binding and rebinding combined lead to a situation in which the virus remains in large part bound to the peptides of the nanoconstructs. H3N2 viruses are also reported to have positively charged hemagglutinin on the surface and therefore to be especially well adapted to bind to negatively charged cell surfaces.<sup>[50]</sup> The negatively charged DNA on the sensor surface and the applied negative DC voltage to the electrodes can have a similar effect of increasing and facilitating the binding interaction of virus and peptide. All of these effects lead to prolonged residence times and therefore influence the calculation of the dissociation rate constant  $k_{\text{off}}$ . Consequently, also the association rate constant  $k_{\text{on}}$  and the dissociation constant  $K_D$ , which both include  $k_{\text{off}}$ , are affected. The measurement was repeated with ss3PeB and ss1PeB. These measurements also lead to a fluorescence signal decrease during association correlating well with the concentration of the X31 virus solution. A quantification to distinguish the binding rate constants for the three structures was not possible in this setup.

As a negative control, ss0PeB (without any peptide) was hybridized and virus solution at a concentration of 40  $\mu\text{g mL}^{-1}$  was injected to check for non-specific binding of X31 virus to the sensor surface or the nanoconstruct. The result shows that the virus only binds specifically to the attached peptides. Unspecific binding onto the surface is not observed (see Figure 5).

The fact that dissociation rate constants are not determinable in this setup is not surprising. The multivalent binding interaction of the virus to the receptors on the sensor surface leads to dissociation times that exceed reasonable measurement times. In general, multivalent binding can be challenging for binding interaction characterization. It has been described also for virus-receptor interactions using surface plasmon resonance (SPR) for the exact case of PeB binding to X31 by Memczak et al.<sup>[35]</sup> Also, there the determination of  $k_{\text{on}}$  and  $k_{\text{off}}$  was not possible. A dissociation constant was determined for the interaction between the peptide and recombinant hemagglutinin protein but not for peptide-virus interactions. Using SPR, a qualitative comparison between variable peptides binding to one virus was possible.

Here, we propose that the DRX<sup>2</sup> can be put to a similar use. We show a strong and specific virus association signal to a

peptide-functionalized surface. Even though we do not calculate rate constants from the data, there is a promising value of a measurement technique that is comparable to SPR. Binding of virus particles to receptors is a common requirement. Furthermore, having the possibility of immobilizing and capturing virus particles on a sensor surface might have additional applications. For example, currently approved anti-viral drugs often target the viral glycoproteins HA and NA, and as mutations can mitigate the efficiency of the drugs, there is a constant need for optimization.<sup>[44]</sup> Our results show that binding interactions of viral glycoproteins can be characterized in vitro in their native environment using a standard biosensor method, which could be utilized as generic tool to characterize, for example, influences of viral mutations on the binding ability.

### 3.2. Sandwich Assay

Immobilization of the virus material on the sensor surface is used in order to find the range of the dissociation constant for the DNA nanoconstructs. We modified the experimental setup as to create a sandwich assay. In this experiment, ss2PeB was hybridized onto the sensor surface. Then, X31 was injected and bound to the ss2PeB. Since nearly no virus dissociation occurred during previous experiments, it was assumed that immobilized viruses remain bound onto the sensor long enough to perform a secondary interaction using the virus surface as capture ligand. Labeling was achieved by hybridization of a complementary DNA tagged with a green fluorophore (G1) prior to the experiment. The fluorescently labeled peptide-construct was injected into the flow channel after virus immobilization and green fluorescence intensity was measured. All of the interaction measurements were carried out in static mode, that is, the DNA nanoconstructs, which tethered the virus to the surface, were subjected to a DC voltage and stayed in an upright position.

A schematic overview of the assay and the results of the binding of ss2PeB-G1 to X31 in the sandwich configuration are shown in Figure 6. The injection of fluorescently labeled DNA-nanoconstructs led to a stepwise increase of fluorescence in the green channel. This step was visible in all injections and

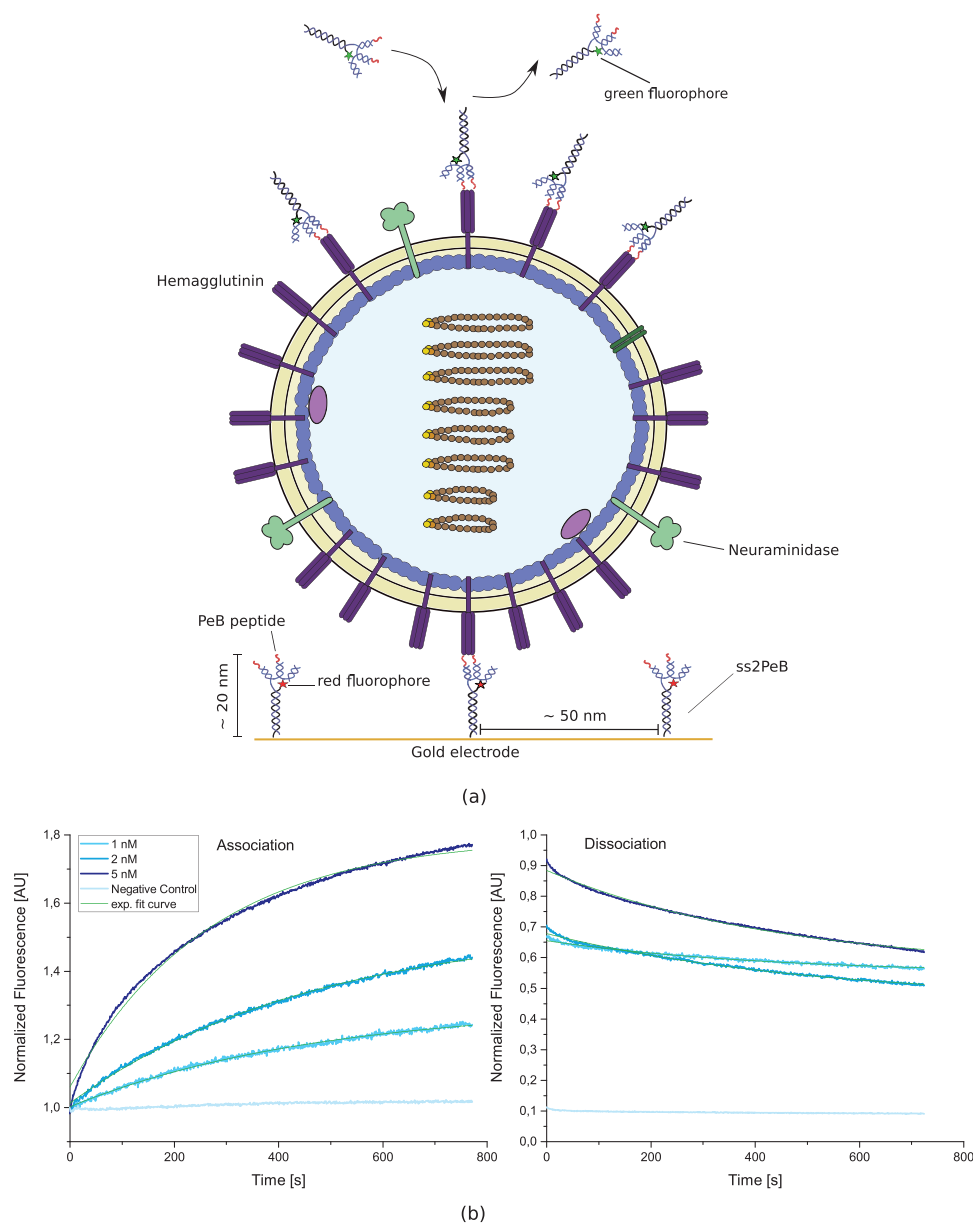


**Figure 6.** a) Schematic overview of the sandwich assay set-up. Virus material was immobilized onto ss2PeB nanoconstructs. Afterward, ss1/2/3PeB was injected that carried a green fluorescence molecule. The DRX<sup>2</sup> device allows independent detection of green and red fluorescence signals. Hence, the stability of virus immobilization was monitored in the red optical channel while peptide binding was detected in the green optical channel. b) Fluorescence signal of sandwich assay: Association of ss2PeB-G1 onto surface-bound X31 virus. Binding of green-labeled constructs to the virus particles was measured by observing accumulation of green fluorescence intensity.

led to a shift in the starting value of the association curve. In general, a very strong signal change was visible during both association and dissociation. A signal increase was measured during association due to the accumulation of labeled nanoconstructs on the sensor surface. By applying the sandwich set-up, it was possible to determine dissociation, since in this orientation the nanoconstructs bound individually onto the virus surface without the previously described cooperative effect of the reverse orientation.

The graphs were fitted using a mono-exponential fit curve and the kinetic parameters for the construct ss2PeB-G1 were

found to be  $k_{on} = (1.8 \pm 0.8) \times 10^5 \text{ M}^{-1} \text{ s}^{-1}$ ,  $k_{off} = (2.3 \pm 0.2) \times 10^{-3} \text{ s}^{-1}$ , and  $K_D = (12 \pm 7) \text{ nM}$  (see Supporting Information for fit formula). The light blue trace shows the negative control. Here, no virus was immobilized to rule out non-specific binding of ss2PeB-G1 onto the sensor surface. The experiments were carried out for fluorescently labeled ss1PeB-G1 and ss3PeB-G1, too. Here, similar signal changes for association and dissociation were obtained. The calculated rate constants were on the same order of magnitude. For ss1PeB-G1, we find  $K_D = (12 \pm 9) \text{ nM}$  and for ss3PeB-G1,  $K_D$  is slightly lower at  $K_D = (8 \pm 7) \text{ nM}$ . The similar  $K_D$  values and large



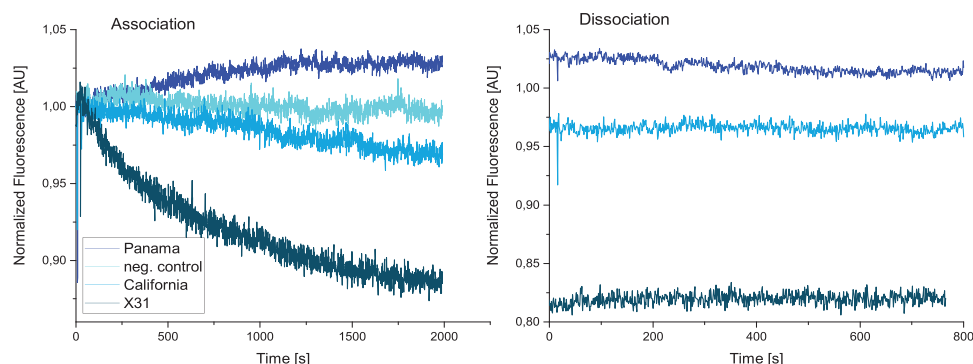


**Figure 7.** Binding of Influenza A/Capifornia/7/2009 (H1N1) and Influenza A/Panama/2007/99 (H3N2) to ss2PeB. As a comparison, the results from a negative control (running buffer) and X31 at  $c = 40 \mu\text{g mL}^{-1}$  are included in the graph.

fit errors complicate a clear comparison between these three constructs. In general, all three of them seem to bind well to the virus surface. The resulting  $K_D$  in the nanomolar range is lower than the one reported by Memczak et al.<sup>[35]</sup> However, that value was determined for the interaction of uncoupled peptide PeB to recombinant hemagglutinin. It is also unclear whether the utilized hemagglutinin was in a monomeric or a trimeric form, which should greatly influence binding strength. Furthermore, dissociation constants in the nM range have been reported for PeB-peptide functionalized polyglycerol-based nanoparticles and X31 viruses in MST measurements by Lauster et al.<sup>[45]</sup> They found that large particle sizes ( $\approx 20\text{--}30$  nm) with a low functionalization density of ligands show the highest affinities. The DNA-peptide nanoconstructs we utilize have a similar size ( $\approx 20$  nm) yet different structure. Still, the multivalent binding that accounts for the improved dissociation constant in the work of Lauster et al. might be similar to our case. The size of the peptide-DNA construct could be beneficial to the binding interaction as well as the negative charge of the DNA backbone. These effects might overshadow the influence of the one, two, or three peptides per construct in this case. Further refinement of experimental and evaluation methods are therefore needed. This could include a direct labeling of the constructs instead of the indirect labeling via DNA-hybridization, a different choice of fluorophore, and a systematic analysis of the step in fluorescence signal at the beginning of the injection of fluorescently labeled DNA-constructs as well as at the end of the measurement when running buffer is injected to measure dissociation. This is necessary to determine the correct start and end-point of the fit curves. The DNA- nanoconstructs could be varied in base pair length as well to quantify the influence of charge and size of the construct on the binding strength. Above that, it would be helpful to simulate the entire binding process in a molecular dynamics simulation. Additionally in this setup, it is more difficult to control the amount of receptors, viruses in this case, on the sensor surface as compared to the original setup in Section 3.1. Still, the results of the sandwich assay confirm the correct and stable immobilization of the X31 viruses on the sensor surface as well as the possibility to measure a second binding interaction using the additional fluorescence channel. A future application of this could be a screening of labeled peptides or antibodies to

virus surface proteins or a comparison of peptide or antibody binding behavior to recombinant viral surface proteins. In prospect of subsequent measurements and developments of this technique in general and the application to virus receptor interactions in particular, this opens the path toward precise and reliable measurements of binding interaction and even oligovalent interactions. The sandwich assay is an important aspect of this.

### 3.3. Variation of Influenza A Subtype/Specificity of PeB

To test the specificity of the peptide PeB, two additional influenza A subtypes were analyzed. Previous studies had shown that the peptide also binds to other subtypes than X31.<sup>[35]</sup> In our experiments, we used influenza A/Capifornia/7/2009 (H1N1) and influenza A/Panama/2007/99 (H3N2) at a concentration of  $c = 40 \mu\text{g mL}^{-1}$  to verify these results using the DRX<sup>2</sup>.

As shown in **Figure 7**, the Panama H3N2 subtype showed a definite increase in fluorescence signal as compared to the negative control. The negative control consists of running buffer. There was only a weak dissociation visible during the measurement of Panama H3N2. The California H1N1 subtype showed a less distinct and weaker signal compared to Panama H3N2. Therefore, it was not possible to conclusively determine whether any binding interaction took place. H1N1 is reported to have a less evolved local positive charge distribution in the HA membrane protein than H3N2.<sup>[50]</sup> Besides the differences in protein structure, this might be a contributing factor to the reduced binding interaction as well.

We see that the PeB also binds other subtypes of influenza A, but less strongly than X31. This confirms the results of the measurements of Memczak et al.<sup>[35]</sup> The peptide was expected to show a broad specificity to influenza A strains to possibly inhibit infections. The hemagglutinin of the subtypes X31 and California 2009 have similar structures in the amino acids that are involved in the peptide binding.<sup>[35]</sup>

The results show that in principle the switchSENSE technique is already suitable to determine qualitative differences in binding strengths of a peptide to various influenza A subtypes. In the future, this will be extended to other receptors as well, like aptamers, antibodies or proteins binding to viruses.

## 4. Conclusion

Our experiments show that the DNA-nanoconstructs are well suited for measurements in the DRX<sup>2</sup> and that virus-peptide interactions can be studied. The peptide PeB coupled to the constructs binds influenza A X31 virus material and a concentration-dependent association signal can be observed using the switchSENSE technology in static mode. The dissociation shows almost no change in the fluorescence signal presumably due to multivalent binding and rebinding effects. In a sandwich assay, we were able to measure concentration-dependent association signals as well as dissociation signals. These signals result in a nanomolar dissociation constant and correspond to the individual dissociation constant for the nanoconstructs. In this configuration, the cooperative, stabilizing effect of multivalent binding between multiple hemagglutinin receptors on the virus surface and several DNA lever arms on the electrode surface was less influential. We were furthermore able to show that the PeB peptide also binds to other Influenza A subtypes. For future investigations, this method could be used to test further variations in the underlying DNA scaffold (e.g., individual arm length, flexibility of the central junction, etc.) in order to better discern the impact that the templated oligovalent presentation has on binding properties. For now, the measurement error was too big to find individual rate constants. In order to find these, far longer dissociation times could be used. The analysis of the specificity of the peptide can also be further investigated by probing more influenza A strains and determining dissociation constants. In general, we show that receptor–virus interactions can be observed using the switchSENSE technology. This first study encountered obstacles that have been known for SPR measurements as well and that need careful consideration. On the experimental side, these are the control of receptor density, influence of mass transport limitations, and sample preparation. The receptor density is controllable by either variation of the number of ssDNA nanolevers on the gold electrode or by quenching of selected fluorophores. The influence of the chip degeneration after experiments, which reduces the amount of the number of available nanolevers, has to be addressed in order to optimize reproducibility. Mass transport limitations can be addressed by reducing the number of receptors and by increasing flow rates. However, reducing the amount of active receptors on the surface has to be balanced with the absolute signal-to-noise ratio of the results. Sample preparation has been challenging as the virus samples loose activity over time. All these effects can influence the measurements and have to be considered in the theoretical analysis. Multivalent binding indicates that mono exponential fit curves might not be appropriate to describe the resulting data. Further theoretical analysis and models might be needed. We decided against applying complicated fit parameters to the direct assay in order to avoid over interpretation of the existing data.<sup>[29]</sup> Very long dissociation times pose an additional problem for theoretical fit analysis. In the sandwich assay, bulk shift reduction would be necessary to account for the shift in fluorescence signal when the fluorophore containing solution reaches the electrode. This is potentially problematic as the complex binding of the three-armed DNA-peptide construct seems to happen strongly and fast to the virus surface, and therefore, the bulk shift may already

include binding signals. Detailed measurements are needed to determine the exact starting and end point of bulk shift effects or whether they can be subtracted from results without influencing calculations of binding constants. The results we present here are a first prove of feasibility to measure virus–receptor interactions, virus immobilization and qualitative comparisons between subtypes and their binding behavior to a peptide on a DNA-based sensor surface.

The future of the applications of this is wide open and can include, for example, peptide optimization, qualitative and possibly quantitative comparison of binding constants of viruses to all kinds of receptors like aptamers, peptides, antibodies, or proteins. Furthermore, the technique can improve the understanding of oligo- and multivalent binding behavior. For this goal DNA-based nanostructures can be applied and varied easily in the DRX<sup>2</sup> that appears to pose an optimal system for this.

Generally, switchSENSE could complement other virus characterization techniques by its easy ability to immobilize full viruses on the surface and hence to target the virus receptors in their native environment on a biosensor.

## Supporting Information

Supporting Information is available from the Wiley Online Library or from the author.

## Acknowledgements

The project “AMBI-SENSE” was supported by the Bundesministerium für Bildung und Forschung as part of the Bio-Chance-Plus/KMU-Innovativ fund. The authors thank Christian Warnt, Sandra Stanke, and Henry Memczak for their help, discussions, and contributions. Furthermore, we thank the Robert Koch Institute for providing the virus material.

Open access funding enabled and organized by Projekt DEAL.

## Conflict of Interest

The authors declare no conflict of interest.

## Data Availability Statement

The data that support the findings of this study are available from the corresponding author upon reasonable request.

## Keywords

binding kinetics, multivalency, switchSENSE technology, virus-peptide interaction

Received: September 6, 2021  
Published online: October 29, 2021

- 
- [1] E. K. McCreary, J. M. Pogue, *Open Forum Infect. Dis.* **2020**, 7, 4.  
[2] A. S. Monto, R. G. Webster, *Influenza Pandemics: History and Lessons Learned*, 2nd ed., John Wiley & Sons, New York **2013**, pp. 20–33.

- [3] D. B. Jernigan, N. J. Cox, *Human Influenza: One Health, One World*, 2nd ed., John Wiley & Sons, New York **2013**, pp. 3–19.
- [4] N. M. Bouvier, P. Palese, *Vaccine* **2008**, *26*, D49.
- [5] J. S. Rossman, R. A. Lamb, *Virology* **2011**, *411*, 229.
- [6] J. Flint, A. M. Skalka, G. F. Rall, V. R. Racaniello, *Principles of Virology*, American Society of Microbiology, Materials Park, OH **2015**.
- [7] X. Xiong, P. J. Coombs, S. R. Martin, J. Liu, H. Xiao, J. W. McCauley, K. Locher, P. A. Walker, P. J. Collins, Y. Kawaoka, J. J. Skehel, S. J. Gamblin, *Nature* **2013**, *497*, 392.
- [8] J. J. Skehel, D. C. Wiley, *Ann. Rev. Biochem.* **2000**, *69*, 531.
- [9] D. K. Takemoto, J. J. Skehel, D. C. Wiley, *Virology* **1996**, *217*, 452.
- [10] N. K. Sauter, J. E. Hanson, G. D. Glick, J. H. Brown, R. L. Crowther, S.-J. Park, J. J. Skehel, D. C. Wiley, *Biochemistry* **1992**, *31*, 9609.
- [11] Y. Horiguchi, T. Goda, A. Matsumoto, H. Takeuchi, S. Yamaoka, Y. Miyahara, *Biosens. Bioelectron.* **2017**, *92*, 234.
- [12] U. Rant, K. Arinaga, S. Fujita, N. Yokoyama, G. Abstreiter, M. Tornow, *Langmuir* **2004**, *20*, 10086.
- [13] U. Rant, K. Arinaga, S. Fujita, N. Yokoyama, G. Abstreiter, M. Tornow, *Nano Lett.* **2004**, *4*, 2441.
- [14] U. Rant, K. Arinaga, M. Tornow, Y. W. Kim, R. R. Netz, S. Fujita, N. Yokoyama, G. Abstreiter, *Biophys. J.* **2006**, *90*, 3666.
- [15] U. Rant, K. Arinaga, S. Fujita, N. Yokoyama, G. Abstreiter, M. Tornow, *Org. Biomol. Chem.* **2006**, *4*, 3448.
- [16] U. Rant, K. Arinaga, S. Scherer, E. Pringsheim, S. Fujita, N. Yokoyama, M. Tornow, G. Abstreiter, *Proc. Natl. Acad. Sci. USA* **2007**, *104*, 17364.
- [17] K. Franz-Oberdorf, A. Langer, R. Strasser, E. Isono, Q. L. Ranftl, C. Wunschel, W. Schwab, *Proteins: Struct. Funct. Bioinf.* **2017**, *85*, 1891.
- [18] I. Ponzio, F. M. Möller, H. Daub, N. Matscheko, *Molecules* **2019**, *24*, 2877.
- [19] A. Langer, W. Kaiser, M. Svejda, P. Schwertler, U. Rant, *J. Phys. Chem. B* **2014**, *118*, 597.
- [20] N. Ferruz, G. D. Fabritius, *Mol. Inf.* **2016**, *35*, 216.
- [21] A. C. Pan, D. W. Borhani, R. O. Dror, D. E. Shaw, *Drug Discovery Today* **2013**, *18*, 667.
- [22] M. Jerabek-Willemsen, T. André, R. Wanner, H. M. Roth, S. Duhr, P. Baaske, D. Breitsprecher, *J. Mol. Struct.* **2014**, *1077*, 101.
- [23] W. Ma, L. Yang, L. He, *J. Pharm. Anal.* **2018**, *8*, 147.
- [24] E. L. Elson, *Biophys. J.* **2011**, *101*, 2855.
- [25] M. Jerabek-Willemsen, C. J. Wienken, D. Braun, P. Baaske, S. Duhr, *ASSAY Drug Dev. Technol.* **2011**, *9*, 342.
- [26] P. J. Tighe, R. R. Ryder, I. Todd, L. C. Fairclough, *PROTEOMICS – Clin. Appl.* **2015**, *9*, 406.
- [27] A. M. Shrivastav, U. Cvelbar, I. Abdulhalim, *Commun. Biol.* **2021**, *4*, 70.
- [28] E. Helmerhorst, D. J. Chandler, M. Nussio, C. D. Mamotte, *Clin. Biochem. Rev.* **2012**, *33*, 161.
- [29] R. L. Rich, D. G. Myszk, *J. Mol. Recognit.* **2008**, *21*, 355.
- [30] D. G. Myszk, *J. Mol. Recognit.* **1999**, *12*, 279.
- [31] A. Langer, M. Schröml, R. Strasser, H. Daub, T. Myers, D. Heindl, U. Rant, *Sci. Rep.* **2015**, *5*, 12066.
- [32] A. Langer, P. A. Hampel, W. Kaiser, J. Knezevic, T. Welte, V. Villa, M. Maruyama, M. Svejda, S. Jähner, F. Fischer, R. Strasser, U. Rant, *Nat. Commun.* **2013**, *4*, 2099.
- [33] J. L. Cuellar-Camacho, S. Bhatia, V. Reiter-Scherer, D. Lauster, S. Liese, J. P. Rabe, A. Herrmann, R. Haag, *J. Am. Chem. Soc.* **2020**, *142*, 12181.
- [34] M. Müller, D. Lauster, H. H. K. Wildenauer, A. Herrmann, S. Block, *Nano Lett.* **2019**, *19*, 1875.
- [35] H. Memczak, D. Lauster, P. Kar, S. D. Lella, R. Volkmer, V. Knecht, A. Herrmann, E. Ehrentreich-Förster, F. F. Bier, W. F. M. Stöcklein, *PLoS ONE* **2016**, *11*, e0159074.
- [36] R. Haag, C. Fasting, C. A. Schalley, M. Weber, O. Seitz, S. Hecht, B. Koks, J. Darnedde, C. Graf, E.-W. Knapp, *Angew. Chem.* **2012**, *124*, 10622.
- [37] H. Yang, P. J. Carney, J. C. Chang, Z. Guo, J. M. Villanueva, J. Stevens, *Virology* **2015**, *477*, 18.
- [38] V. Bandlow, S. Liese, D. Lauster, K. Ludwig, R. R. Netz, A. Herrmann, O. Seitz, *J. Am. Chem. Soc.* **2017**, *139*, 16389.
- [39] M. Yamabe, K. Kaihatsu, Y. Ebara, *Bioorg. Med. Chem. Lett.* **2019**, *29*, 744.
- [40] M. Yamabe, K. Kaihatsu, Y. Ebara, *Bioconjugate Chem.* **2018**, *29*, 1490.
- [41] M. Yamabe, A. Fujita, K. Kaihatsu, Y. Ebara, *Carbohydr. Res.* **2019**, *474*, 43.
- [42] D. M. Smith, J. S. Lorenz, C. Möser, J. Fertey, W. Stöcklein, A. Herrmann, D. Lauster, WO 2018/215660 A1, **2018**, <https://patentimages.storage.googleapis.com/49/75/27/5efe02b1905260/WO2018215660A1.pdf>.
- [43] D. Smith, C. Möser, T. Grunwald, L. Mail, C. Jäger, M. Kleinschmidt, D. Ramsbeck, M. Buchholz, WO 2020/212576 A1, **2020**, <https://patentimages.storage.googleapis.com/38/57/28/c69c84866f848f/WO2020212576A1.pdf>.
- [44] N. A. Ilyushina, T. E. Kornatsu, W. L. Ince, E. F. Donaldson, N. Lee, J. J. O'Rear, R. P. Donnelly, *Virol. J.* **2019**, *16*, <https://doi.org/10.1186/s12985-019-1258-x>.
- [45] D. Lauster, M. Glanz, M. Bardua, K. Ludwig, M. Hellmund, U. Hoffmann, A. Hamann, C. Böttcher, R. Haag, C. P. R. Hackenberger, A. Herrmann, *Angew. Chem., Int. Ed.* **2017**, *56*, 5931.
- [46] H. Müller-Landau, P. F. Varela, *European Biophysics Journal* **2021**, *50*, 389.
- [47] C. Möser, J. Lorenz, M. Sajfutdinow, D. Smith, *Int. J. Mol. Sci.* **2018**, *19*, 3482.
- [48] T. M. Squires, R. J. Messinger, S. R. Manalis, *Nat. Biotechnol.* **2008**, *26*, 417.
- [49] M. R. Eftink, *Fluorescence Quenching: Theory and Application*, Kluwer Academic Publishers, Dordrecht, The Netherlands **2002**, pp. 53–120.
- [50] C. M. Saad-Roy, N. Arinaminpathy, N. S. Wingreen, S. A. Levin, J. M. Akey, B. T. Grenfell, *PLoS Comput. Biol.* **2020**, *16*, e1007892.